

PHOTONICS Research

Compact seven-core fiber spatiotemporal mapping system for spatiotemporal mode-locking buildup dynamics

YU NING,¹ JIANGYONG HE,^{1,2} JIN LI,¹ YUANSHENG MA,¹  SHIHAI WANG,¹ ZHEZHE LI,¹ MINGTONG XIAO,¹ LINGYU SHEN,¹ ZHI WANG,^{1,3} AND YANGE LIU¹ 

¹Institute of Modern Optics, Nankai University, Tianjin Key Laboratory of Micro-scale Optical Information Science and Technology, Tianjin 300350, China

²e-mail: 9820220043@nankai.edu.cn

³e-mail: zhiwang@nankai.edu.cn

Received 25 November 2024; revised 1 April 2025; accepted 28 April 2025; posted 28 April 2025 (Doc. ID 549612); published 1 July 2025

Effective detection schemes for spatiotemporal light fields hold significant importance in the study of high-dimensional spatiotemporal nonlinear systems. We propose a compact seven-core fiber spatiotemporal mapping system (SCF-SMS) to investigate the transient dynamics within a spatiotemporal mode-locked (STML) fiber laser. By utilizing this system, we observed intriguing transient phenomena during STML processes, including beating dynamics and spatiotemporal soliton state transition dynamics. In the beating dynamics, two channels corresponding to distinct spatial sampling points exhibited different transient behaviors. Conversely, during the spatiotemporal soliton state transition dynamics, the transition processes of two channels were asynchronous, with observable discrepancies before and after the transitions. Compared with existing spatiotemporal light field acquisition methods, the SCF-SMS enables more compact spatiotemporal mapping within STML fiber lasers. This real-time, synchronous system for spatiotemporal soliton information measurement facilitates an in-depth study of nonlinear dynamical phenomena in STML fiber lasers. © 2025 Chinese Laser Press

<https://doi.org/10.1364/PRJ.549612>

1. INTRODUCTION

Multimode fiber (MMF) has attracted widespread attention in optical communications owing to its ability to support a larger information capacity and higher pulse energy [1–3]. Compared with single-mode fiber (SMF), the incorporation of spatial dimensions in MMF enables the exploration of high-dimensional spatiotemporal nonlinear dynamics, which are of great significance for the theoretical study of nonlinear fiber optics [4,5]. Over the past decade, research on MMF has encompassed investigations into multimode solitons [6,7], spatiotemporal instability [8–10], wavefront shaping of multimode nonlinear waves [11,12], and beam self-cleaning [13,14]. In 2017, a passively mode-locked fiber laser based on graded-index (GRIN) MMF was proposed, achieving simultaneous locking of transverse (spatial) and longitudinal (temporal) modes, which is known as a spatiotemporal mode-locked (STML) fiber laser [15]. In contrast to single-mode passively mode-locked fiber lasers, the STML fiber lasers can generate higher-energy pulses and higher-order spatial modes. It not only provides an excellent experimental platform for investigating the nonlinear dynamics phenomena in MMF [16–18], but also promotes

the development of high-dimensional nonlinear optical theory [19,20].

In recent years, the physical mechanisms and nonlinear dynamic phenomena in STML fiber lasers have been extensively investigated. Researchers have established attractor analysis models and mother-child coupling models to simulate and analyze the underlying physical mechanisms in spatiotemporal mode-locking [15,20,21]. Additionally, many intriguing nonlinear dynamical phenomena have been observed in experiment such as spatiotemporal self-similar solitons [22], multiple solitons [23,24], soliton molecules [25,26], *Q*-switching/mode-locking switching [27], and spatiotemporal period-doubling bifurcation [28]. However, the complex three-dimensional soliton dynamics emerging from multidimensional random seeds exhibit unpredictable, time-variant, and non-reproducible characteristics, posing significant challenges for systematic analysis [29]. Consequently, there is a critical demand for spatiotemporal light field measurement techniques with high resolution and real-time synchronous sampling capabilities, particularly for capturing transient processes during the formation of complex dynamic phenomena. Existing methods for measuring spatiotemporal light fields include delayed scanning

off-axis digital holography [30], Michelson interferometer time scanning full electric field reconstruction [31], compressed ultrafast time spectral photography [32], single-lens compressed ultrafast photography [33], and multi-exposure frequency recognition algorithms based on laser probes [34]. These methods struggle to simultaneously balance the spatiotemporal resolution and real-time synchronization. In 2021, Guo *et al.* proposed a multi-speckle real-time synchronous time-frequency observation system, which overcomes the problems of real-time synchronization and recording frame rate [35]. Nevertheless, this detection system necessitates multiple beam collectors and beam splitters (BSs) for speckle pattern acquisition, requiring the construction of expensive and complex optical detection systems.

In this work, we present a compact seven-core fiber spatiotemporal mapping system (SCF-SMS) for investigating transient establishment dynamics during spatiotemporal mode-locking. The system comprises an SCF fan-out module and a time-stretch module. The SCF fan-out is constructed of SCF and seven SMFs with high-power coupling. The output light field of the STML fiber laser is sampled using the SCF fan-out module. Subsequently, the collected signals are fed into a dispersion-compensating fiber (DCF) for stretching, in conjunction with the time stretching dispersion Fourier transform (TS-DFT) technology [36,37], to achieve spatiotemporal mapping. As an all-fiber structure, this system overcomes the real-time and synchronization limitations of three-dimensional light field sampling, making it more compact and convenient. We observed two intriguing stages during the establishment process of spatiotemporal mode-locking, including beating dynamics and spatiotemporal soliton state transition dynamics. We found that during these two stages, different spatial sampling points exhibit distinct transient behaviors and observable evolutionary spectrum discrepancies before and after the transitions. This finding validates the effectiveness of SCF-SMS. It provides new insights into the means of detecting three-dimensional spatiotemporal light fields and helps to explore more nonlinear dynamical phenomena within STML fiber lasers.

2. EXPERIMENT SETUP

A. Characteristics of SCF-SMS

The key component of the SCF-SMS is a specialized multi-core fiber (MCF), which is designed with multiple independent cores within a shared cladding area. The end face of the SCF is shown in Fig. 1(a). The core diameter is 8 μm , the core spacing is 41.5 μm , and the cladding diameter is 150 μm . By using a fluorine doped cladding refractive index distribution structure, the SCF and seven SMFs achieved high-power coupling with low insertion loss (<1.5 dB), low inter core crosstalk (<-50 dB), and high return loss (>45 dB) based on a conical process, and were prepared as the SCF fan-out module. This module, together with the time-stretch module based on TS-DFT technology, constitutes an SCF-SMS. It can realize real-time synchronous mapping of spectral-spatial-temporal information with STML fiber lasers, and is used to analyze the mode-locking transient establishment process in this paper.

As is well known, the output light field of the STML fiber lasers is typically represented as a speckle with complex spatial

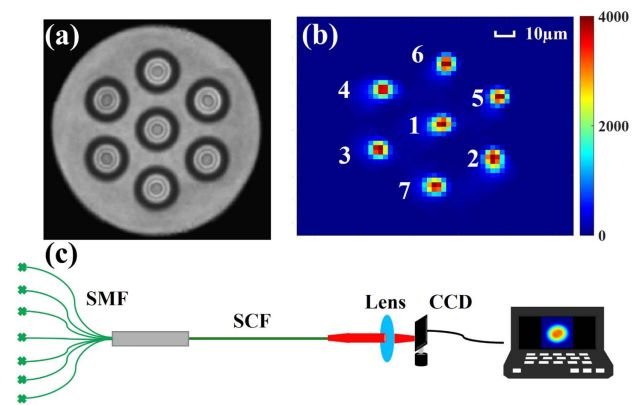


Fig. 1. Schematic diagram of sampling performance test of SCF fan-out module. (a) The cross section of SCF. (b) The sampling result of SCF fan-out module. (c) The experimental device diagram for testing the sampling capacity of SCF fan-out module. SCF: seven-core fiber. CCD: charge-coupled device.

energy distribution [9,10]. We first tested the sampling capacity of the SCF fan-out module as shown in Fig. 1(c). In this experiment, seven SMFs are used as input ports, while the MCF serves as the output port. We employ a 1030 nm fiber laser as the light source, sequentially injecting light into the seven pre-labeled SMFs. The light field distribution at the SCF was collected using a lens and a charge-coupled device (CCD), as depicted in Fig. 1(b). The numbers represent pre-labeled SMF channels. The positional distribution of the light spots demonstrates that the SMF collected seven different spatial positions corresponding to the SCF end face, and the energy distribution shows that the spots are well confined within the fiber core. In addition, the fiber core spacing is much larger than the girdle radius of a single spot, so the crosstalk of the SCF is almost negligible. This validates the effectiveness of the SCF fan-out module as a spatiotemporal light field sampling tool.

B. Spatiotemporal Mode-Locking

The schematic diagram of the STML fiber laser and SCF-SMS is shown in Fig. 2. The STML fiber laser was backward pumped by a 980 nm pump source through a 980/1030 nm combiner. The pump light was injected into a 1.2 m long double-clad ytterbium doped gain fiber (Liekki YB1200-10/125DC) as the gain medium of the laser, and then the gain fiber was spliced with a Corning SMF-28e fiber (9/125). Three modes including LP_{01} , LP_{11} , and LP_{21} were excited when the 1030 nm laser light was injected into the gain fiber and SMF. The SMF was embedded with a double-resonance-coupled long-period fiber grating (LPFG) to compensate for mode dispersion, allowing interconversion between LP_{01} and LP_{11} in the cavity [38,39]. Afterwards, the output light of the SMF was collimated by lenses L1, L2 and formed a spatial loop feedback with the help of mirrors M1, M2. In the spatial optical path, a spectral filter (SF) with center wavelength of 1030 nm and 3 dB bandwidth of 10 nm was incorporated for spectral filtering. The saturable absorber based on the nonlinear polarization rotation (NPR) effect is composed of a half-wave plate (HWP), a polarization dependent isolator (PD-ISO), and

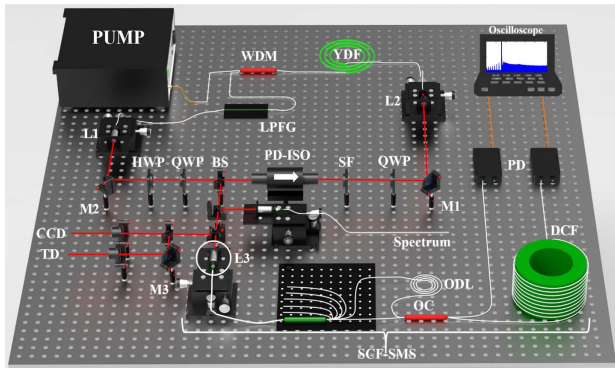


Fig. 2. Schematic diagram of STML laser and SCF-SMS. Pump: 980 nm laser diode. WDM: wavelength division multiplexer. LPFG: long-period fiber grating. L1, L2, L3: lenses. M1, M2, M3: mirrors. HWP: half-wave plate. QWP: quarter-wave plate. BS: beam splitter. PD-ISO: polarization-dependent isolator. SF: spectral filter. ODL: optical delay line. OC: optical coupler. DCF: dispersion compensating fiber. PD: photodetector.

two quarter-wave plates (QWPs). With the assistance of SF and spatial coupling, modal dispersion and chromatic dispersion within the cavity were compensated for, resulting in spatiotemporal mode locking [40–42]. The output of the laser was split by a BS with a power ratio of 70:30, and 30% of the laser was directed into the SCF-SMS for detection.

The 30% split laser output from the STML fiber laser was coupled via L3 to the end face of the SCF fan-out module, as illustrated in the white circle in Fig. 2. All SMFs can serve as spatial probes to obtain mapped information under the same STML state; we selected two channels with high coupling power to investigate the buildup transient dynamics process at spatiotemporal mode-locking. Two channels are labeled as channel II and channel VII, respectively corresponding to marker 2 and marker 7 in Fig. 1(b). The spatial light field information mapped to two channels through the SCF fan-out module was time-division multiplexed via a 3 m optical delay line (ODL) (approximately half a cavity roundtrip), and then combined into a 50:50 optical coupler (OC). The multiplexed information from the two channels was divided into two paths. One path connected to a 1 km DCF [G.652 C/250, dispersion -77.24 ps/(nm · km)] for dispersion stretching. The signal was converted into an electrical signal by a 40 GHz photodetector (PD1, Aoshow Information, HSPD4040) and measured in real-time spectral evolution by using a high-speed oscilloscope (Tektronix DPO75902SX) with a bandwidth of 33 GHz and a sampling rate of 200 GS/s. The other path was acquired by a photodetector (PD2, Keyang Photonics, KY-PRM-I-FA) with a bandwidth of 18 GHz and a high-speed oscilloscope to detect real-time pulse sequence evolution. The spectrum and light field at the STML state were obtained by a spectrometer (OSA, Yokogawa AQ6370D, 0.02 nm) and a CCD (Beam on U3).

3. RESULT AND DISCUSSION

When the pump power was adjusted to 3.4 W, the laser achieved stable mode locking by rotating the HWP and QWP. The 30% output signal split from BS during mode

locking was approximately 200 mW. The basic characteristics of the STML laser are depicted in Fig. 3. The spectrum of spatiotemporal mode-locking is shown in Fig. 3(a), with the 3 dB bandwidth of approximately 12 nm. Figure 3(b) illustrates the laser operating in a dual-soliton state with a pulse interval of 30.65 ns, corresponding to the repetition frequency of 32.63 MHz in Fig. 3(c); the signal-to-noise ratio is 55.23 dB. The overall cavity length of the laser is 6.14 m. The output light field is shown in Fig. 3(d), which presents a double-lobe pattern with one lobe having higher energy. Since the LPFG was incorporated in the cavity to compensate for inter-mode dispersion, this suggests that the modes in the cavity during the spatiotemporal mode-locking were LP_{01} and LP_{11} , and that LP_{11} had a higher composition. The total power of the output laser coupled to the seven-core fiber fan-out module was 5 mW. The powers of channel II and channel VII, which correspond to the sampling points at the white triangular markers in Fig. 3(d), were 1.8 mW and 1.2 mW, respectively. The coupling efficiency was 2.5%. The signal power was reduced to 1.5 mW with an insertion loss of 3 dB after the two channels had been combined by 50/50 OC combining, which cannot be avoided with time-division multiplexing. The spectra of the two channels are depicted in Fig. 4(a), which indicated that mode locking was achieved at different sampling positions and the laser reached the STML state. The comparison of the average spectra measured by the spectrometer and the evolved spectra after TS-DFT of channel II is depicted in Fig. 4(b). Limited by the detector bandwidth, the actual resolution of the TS-DFT is 0.32 nm, which cannot map all the details in the averaged spectrum, but its overlapping overall profile suggests that the SCF-SMS can realize the spatiotemporal mapping of the two acquisition channels.

A. Building Dynamics of Spatiotemporal Mode-Locking

With the help of the SCF-SMS system, we analyzed the transient establishment process of spatiotemporal mode-locking, as

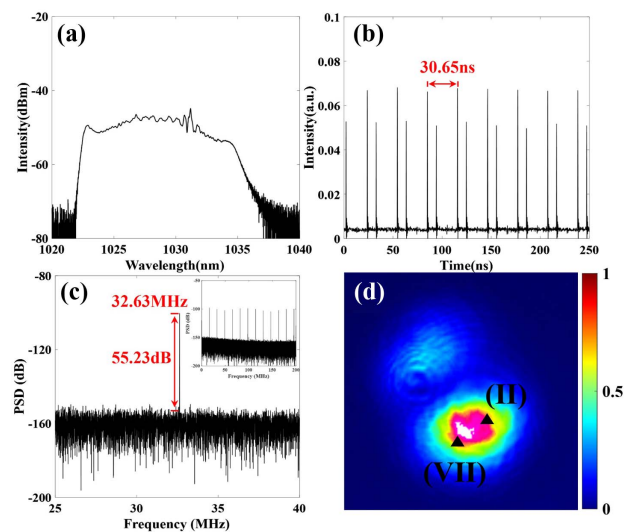


Fig. 3. The basic characteristics of spatiotemporal mode-locking. (a) The spectrum. (b) Time domain pulses. (c) The RF spectrum. (d) The light fields (the black triangular markers correspond to the two acquisition channels).

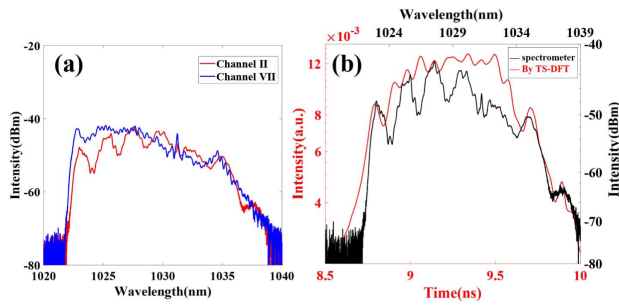


Fig. 4. (a) The comparison of average spectra by spectrometer between two channels. (b) The comparison of average spectra by spectrometer and evolution spectra by TS-DFT in channel II.

shown in Fig. 5. The waveforms of the data collected after time-division multiplexing of two channels are shown in Fig. 5(a). The two-dimensional contour map of two channels ranging over 10,000 roundtrips is depicted in Fig. 5(b). The establishment of spatiotemporal mode-locking underwent four distinct stages, (i) *Q*-switching [43], (ii) beating dynamics, (iii) spatiotemporal soliton state transition dynamics, and (iv) stable dual-soliton. The black arrows in Fig. 5(a) delineate these stages. The enlarged detail of the white dashed box in Fig. 5(b) is illustrated in Figs. 5(c) and 5(d), which clearly distinguish the differences in the establishment process of spatiotemporal mode-locking between two channels. Figure 5(e) shows the average mapping spectrum of two channels within stage iv (after 7000 roundtrips). The difference in the profiles of the average spectra indicated that two channels collected dual-soliton pulses with different transverse mode components. The detailed diagram of the *Q*-switching process is displayed in Fig. 5(f). The total energy evolution of the two channels in Fig. 5(b) is depicted in Figs. 5(g) and 5(h). The illustration in the upper right corner is the detailed diagram in the black dashed box during stage ii.

From the evolution process of the two channels in Fig. 5(b), there is a clear *Q*-switching stage in the establishment of spatiotemporal mode-locking, with a *Q*-switching pulse time interval of 10.47 μ s, corresponding to a repetition frequency of 93.10 kHz. Comparing the first 2800 roundtrips in Fig. 5(f), we observed that the intensity of the *Q*-switching pulses and the sparse spacing between the pulses are periodic in the first five *Q*-switching cycles. The *Q*-switching pulses in the first cycle transition from a low repetition rate with high intensity to a high repetition rate with low intensity, and then cycle until the fifth cycle. Subsequently, the periodicity disappears as the mode-locked pulses are generated. This interesting phenomenon may be attributed to the different linearities and different phase shifts of the distinct modes in the cavity, inducing a short periodic rotation of the optical field, leading to overlapping and interleaving of the *Q*-switching pulses collected by the two channels. Afterwards, the two channels underwent a stage of differential beating dynamics. The details of the energy variation in the insets of Figs. 6(g) and 6(h) validate the differences (details as described in Section 3.B). During the spatiotemporal soliton state transition dynamics, the dual-solitons of two channels drift, due to the fact that the group velocities of the different transverse modes are not yet bound during the

mode-locking establishment process [20]. This is followed by entry into the spatiotemporal soliton state transition (details as described in Section 3.C). Finally, the dual-soliton from both channels reached a stable state, and the laser achieved stable spatiotemporal mode locking. We analyze the two transition states in detail below.

B. Beating Dynamics

The detailed slice evolution during the beating dynamics at the STML state is depicted in Fig. 6. During the RT2500 to RT2570, the multiple subnanosecond pulses coexist inside the cavity, which is considered a marker of the occurrence of beating dynamics. Then, a few subnanosecond pulses in channel II dominated and underwent a drastic change in energy, evolving into a mode-locked pulse, labeled as hybrid mode pulse i and hybrid mode pulse ii. Similar behavior also occurred in channel VII. The white dashed lines in Fig. 6(a) mark the three stages of subnanosecond pulses evolving into mode-locked pulses, while Figs. 6(b) and 6(c) display the beating dynamic enlarged details of the two channels. The single-shot spectra of the two channels in the three stages marked by white dashed lines are illustrated in Figs. 6(d) and 6(e). The subnanosecond pulses of both channels undergo significant energy changes at RT2560, followed by noticeably broadened evolutionary spectra at RT2600. Additionally, the hybrid mode pulse i and hybrid mode pulse ii, both in channel II, have an asynchronous relationship, with hybrid mode pulse i being established 40 roundtrips (1.2 μ s time interval) earlier than hybrid mode pulse ii. In the hybrid mode pulse iv of channel VII, the subnanosecond pulses underwent pulse splitting before forming a mode-locked pulse, as illustrated by the white dashed circle in Fig. 6(c). This split small pulse appeared at RT2570 and gradually reduced in energy until it completely annihilated at RT2600. At the same time, there is no such behavior in channel II in Fig. 6(b). In the upcoming transition to stage iii, the evolution spectra of the two channels exhibited disparity. The spectrum of hybrid mode pulse iv shows a distinct two-peak structure compared to hybrid mode pulse ii in Fig. 6(e), which may be caused by pulses splitting at RT2600. The different evolutionary behaviors of the mode-locked pulse during beating dynamics confirm that the SCF-SMS collects distinct mode-locked transient establishment processes.

C. Spatiotemporal Soliton State Transition Dynamics

The detailed slicing evolution processes during the spatiotemporal soliton state transition dynamics are depicted in Fig. 7. The pulse evolution within two channels during the spatiotemporal soliton transition state dynamics is illustrated in Fig. 7(a). The magnified details of the transient process in the white dashed box are shown in Figs. 7(b) and 7(c). The apparent fluctuation within both channels indicated that the pulses underwent spectral broadening and narrowing before transitioning to stable dual-solitons. This phenomenon is similar to soliton pulsation behavior.

We performed the single-shot slicing on the spectra at the broadening and narrowing stage of the four hybrid mode pulses, as illustrated in Figs. 7(d) and 7(e). From the blue dashed box marked in the single-shot spectra, the fluctuations of pulses correspond to the evolution of adjacent edge peaks of

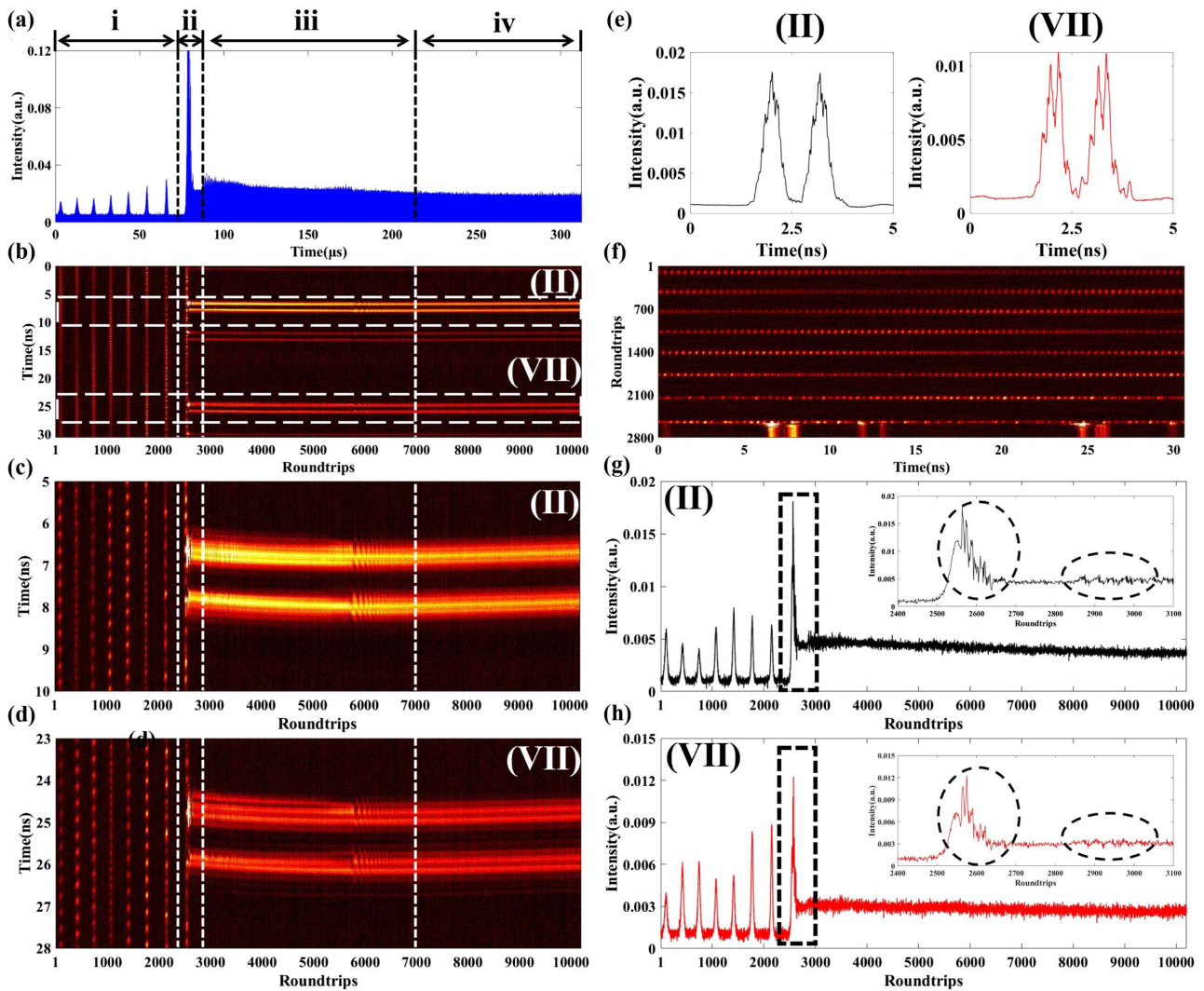


Fig. 5. The transient establishment dynamics of spatiotemporal mode-locking within two channels. (a) The transient establishment data acquired from two channels by time-division multiplexing. The black solid and dashed lines delineate the four stages in the establishment process of spatiotemporal mode-locking: (i) *Q*-switching, (ii) beating dynamics, (iii) spatiotemporal soliton state transition dynamics, and (iv) stable dual-soliton. (b) Two-dimensional contour map of accumulated data ranging over 10,000 roundtrips (the pulses outside the white dashed box are the higher-order mode pulses due to the 1030 nm laser injection into the 1550 nm stretched fiber, which do not affect the evolutionary characteristics of the STML buildup process, so we have ignored this part in the subsequent studies). (c), (d) The enlarged details within the white dashed box in (b), and the white dashed line also marks the four stages. (e) The average mapping spectrum of two channels within stage iv. (f) The detailed diagram of the *Q*-switching process. (g), (h) The total energy evolution corresponding to two channels. The inset shows the enlarged energy variation during stage ii (indicated by the black dashed rectangle).

both hybrid mode pulses. At RT5868 in Fig. 7(b), the evolutionary spectrum of hybrid mode pulse i in channel II expanded to a maximum, while the evolutionary spectrum of hybrid mode pulse ii in the same channel shrank to a minimum. In contrast, this behavior is just the opposite at RT5938 in Fig. 7(c). Reflected in Fig. 7(d), the generation and suppression of adjacent edge peaks of two hybrid mode pulses can be observed. This phenomenon indicates that there is a spatiotemporal interaction between two hybrid mode pulses within channel II, inducing asynchronous soliton pulsations [44]. Similar behavior also exists in channel VII, and the variation of edge peaks in the single-shot spectra is more pronounced than in channel II. In addition, when the spectral width of the

two hybrid mode pulses in channel II reached its limit, the two hybrid mode pulses in channel VII did not reach the extreme value of the spectral widths, which indicates that the asynchronous pulsation process in both channels was also asynchronous. We zoom in on this slice evolution of pulsation behavior in detail, as depicted in Figs. 8(a) and 8(b). Typical soliton pulsation occurred in both channels, which confirms that the soliton pulsations can be established in STML fiber lasers between *Q*-switching and stable mode locking. The overall energy evolution and enlarged details of four hybrid mode pulses during pulsation behavior are shown in Figs. 8(c) and 8(d). The two hybrid mode pulses, both in a single channel, exhibited asynchronous double-period pulsation. This pulsation behavior

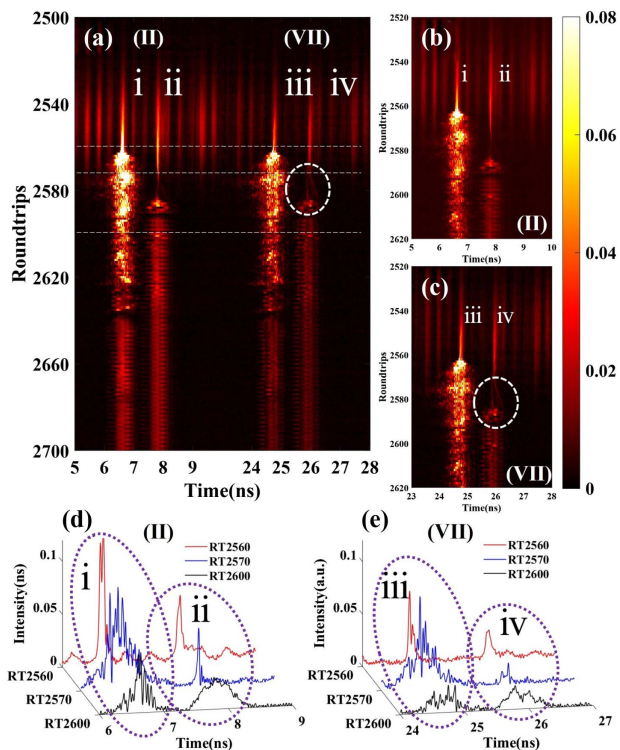


Fig. 6. The beating dynamics of spatiotemporal mode-locking. (a) The evolution of two-dimensional contour map of beating dynamics process. (b), (c) The beating dynamic enlarged details of channels II and VII. (d) The single-shot spectra of hybrid mode pulses i and ii at the white dashed line markers. (e) The single-shot spectra of hybrid mode pulses iii and iv at the white dashed line markers (the purple dashed box was used to compare the pulse details).

has been shown to be caused by the spatiotemporal interactions of different modes within STML fiber laser [45].

We further analyze the phase-space evolution of the four hybrid mode pulses during the pulsation process [46]. The phase-space of the intensities and phases at fixed points in the autocorrelation for each roundtrip of four hybrid mode pulses was used to reflect the evolutionary differences in the real-time spectra. As shown in Fig. 9, the complexity of the phase-space of each hybrid mode pulse and the differences in the phase-space evolution characteristics of different hybrid mode pulses indicate that the spectra of the four hybrid mode pulses exhibit a differentiated evolution during the spatiotemporal soliton state transition. Finally, when the laser reached stable mode locking, the real-time evolution spectrum of hybrid mode pulses in channel II has a single-peak structure, while channel VII shows a double-peak structure. These differences are sufficient to demonstrate that the two channels collect distinct STML building processes. This observation confirms the spatial sampling capability and real-time synchronization performance of the SCF-SMS.

Due to the spatial coupling between the light field distribution of the output from the STML fiber laser and the end face of the SCF, a small portion of the mode information may not be collected into the SMF as the output end, which may result in the loss of details on the impact of mode interaction between

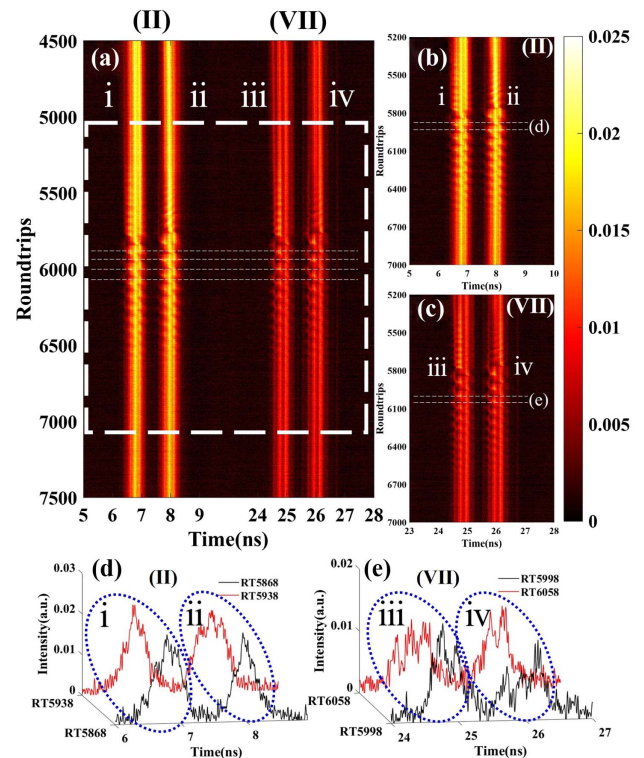


Fig. 7. Spatiotemporal soliton state transition dynamics of spatiotemporal mode-locking. (a) The slice evolution of spatiotemporal soliton state transition during the process of establishing spatiotemporal mode-locking. (b), (c) The detail display of the white dashed box in (a). (d) The single-cycle evolution spectrum marked by white dashed line markers in (b). (e) The single-cycle evolution spectrum marked by white dashed line markers in (c) (the blue dashed box was used to compare the pulse details).

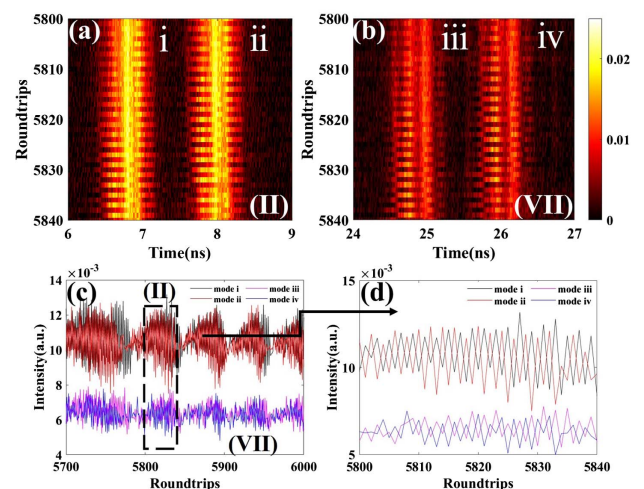


Fig. 8. The slice evolution of pulsation soliton in detail. (a) The slice evolution of pulsation behavior of channel II from RT5800 to RT5840. (b) The slice evolution of pulsation behavior of channel VII from RT5800 to RT5840. (c) The overall energy evolution of four hybrid mode pulses during pulsation. (d) The energy details in the black dashed box in (c).

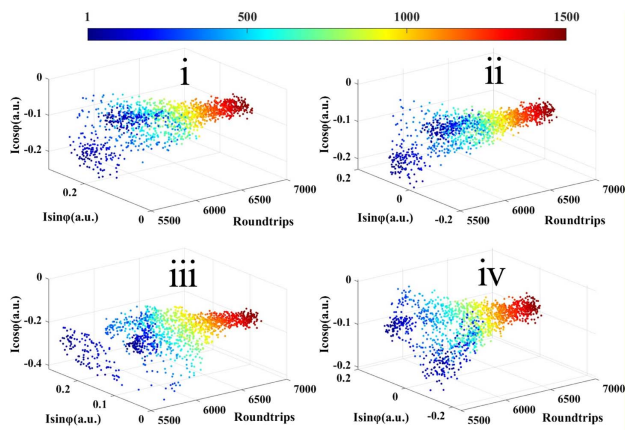


Fig. 9. The phase-space of the intensities and phases at fixed points in the autocorrelation for each roundtrip of four hybrid mode pulses during spatiotemporal soliton state transition dynamics.

multiple transverse modes [35]. Higher-order modes are inevitably generated due to the wavelength mismatch between the operation of the SCF-SMS and the STML fiber laser. However, the effect of higher-order modes is negligible in the time domain of lasers with a cavity period of only 30 ns. And in the 1550 nm DFT module, such higher-order modes can be completely separated, which does not have any effect on our probing of the dynamical processes of established spatiotemporal mode-locking, and does not affect the feasibility and innovativeness of the system as a probe of the three-dimensional spacetime light field.

Furthermore, in this work, we have used the SCF-SMS to discover commonalities between STML fiber lasers and single-mode lasers in the buildup process, such as beating dynamics [43]. In future work, we aim to enhance the detection system to maximize the collection of mode field distribution information. Additionally, we will focus on demultiplexing and analyzing the complex spatial superposition of light field data [47]. This is crucial for understanding the mechanisms underlying the establishment of spatiotemporal mode-locking.

4. CONCLUSION

The STML fiber laser, as a high-dimensional platform, has important research significance for exploring high-dimensional spatiotemporal nonlinear dynamics and enriching the theoretical system of nonlinear fiber optics. However, the measurement systems with real-time synchronized measurement performance have often increased the cost and complexity. There is an urgent need for a compact measurement system that can achieve real-time synchronized spatiotemporal information mapping of nonlinear dynamics in the STML fiber laser, and further study the physical mechanism of multi-mode fiber nonlinear dynamics systems.

We proposed a compact SCF-SMS for real-time synchronized analysis of the three-dimensional light field output by STML fiber lasers. An SCF-SMS with an all-fiber structure was prepared by coupling SCF and seven SMFs by using a tapered process with low loss, low crosstalk, and high coupling efficiency. The system collects the output light field of the

STML fiber laser into SMFs corresponding to different spatial positions. Then, in combination with the TS-DFT technology, the real-time spatiotemporal mapping of the establishment dynamics in STML fiber lasers was achieved. We observed that in the initial establishment process of spatiotemporal mode-locking, there are two processes: beating dynamics and spatiotemporal soliton state transition dynamics, which have not been mentioned in previous studies on establishment dynamics of STML fiber lasers. We found that two channels corresponding to different spatial sampling points exhibit distinct transient behaviors in beating dynamics, and induce real-time spectral evolution differences of stable mode-locked pulses. During the spatiotemporal soliton state transition dynamics, two hybrid mode pulses in the same channel exchange energy due to spatiotemporal interactions, resulting in soliton pulsation behavior. The hybrid mode pulses of two channels exhibit obvious asynchrony and observable evolutionary spectrum variation before and after the transitions. These differences demonstrate the excellent detection performance of the SCF-SMS. Compared with existing spatiotemporal light field acquisition methods such as multi-speckle spatial probe methods, this system reduces the cost of detection devices and the complexity of building detection devices, and realizes real-time synchronized spatiotemporal mapping more compactly and conveniently. The proposed system helps to explore the evolution of spatiotemporal solitons, which is important for understanding the nonlinear dynamics phenomena of spatiotemporal solitons in STML fiber lasers and provides a new feasibility for the probing scheme of three-dimensional spatiotemporal light fields.

Funding. National Natural Science Foundation of China (12274238, 62205159, 61835006); Natural Science Foundation of Tianjin Municipality (19JCZDJC31200); Special Project for Cooperation in Basic Research of Beijing, Tianjin and Hebei (21JCZJJC00010).

Disclosures. The authors declare no conflicts of interest.

Data Availability. Data underlying the results presented in this paper are not publicly available at this time but may be obtained from the authors upon reasonable request.

REFERENCES

1. L. G. Wright, F. O. Wu, D. N. Christodoulides, *et al.*, "Physics of highly multimode nonlinear optical systems," *Nat. Photonics* **18**, 1018–1030 (2022).
2. L. G. Wright, W. H. Renninger, D. N. Christodoulides, *et al.*, "Nonlinear multimode photonics-nonlinear optics with many degrees of freedom," *Optica* **9**, 824–841 (2022).
3. M. A. Eftekhar, Z. Sanjabi-Eznaveh, H. E. Lopez-Aviles, *et al.*, "Accelerated nonlinear interactions in graded-index multimode fibers," *Nat. Commun.* **10**, 1638 (2019).
4. K. Krupa, A. Tonello, A. Barthelemy, *et al.*, "Multimode nonlinear fiber optics, a spatiotemporal avenue," *APL Photonics* **4**, 110901 (2019).
5. B. Fu, C. Shang, H. Y. Liu, *et al.*, "Recent advances and future outlook in mode-locked lasers with multimode fibers," *Appl. Phys. Rev.* **10**, 041305 (2023).
6. L. G. Wright, W. H. Renninge, D. N. Christodoulides, *et al.*, "Spatiotemporal dynamics of multimode optical solitons," *Opt. Express* **23**, 3492–3506 (2015).

7. W. H. Reninger and F. W. Wise, "Optical solitons in graded-index multimode fiber," *Nat. Commun.* **4**, 1719 (2013).
8. R. Dupiol, A. Bendahmane, K. Krupa, *et al.*, "Intermodal modulational instability in graded-index multimode optical fibers," *Opt. Lett.* **42**, 3419–3422 (2017).
9. K. Krupa, A. Tonello, A. Bendahmane, *et al.*, "Observation of geometric parametric instability induced by the periodic spatial self-imaging of multimode waves," *Phys. Rev. Lett.* **116**, 199902 (2016).
10. L. G. Wright, Z. W. Liu, D. A. Nolan, *et al.*, "Self-organized instability in graded-index multimode fibres," *Nat. Photonics* **10**, 771–776 (2016).
11. O. Tzang, A. M. Caravaca, K. Wagner, *et al.*, "Adaptive wavefront shaping for controlling nonlinear multimode interactions in optical fibres," *Nat. Photonics* **12**, 368–374 (2018).
12. X. M. Wei, J. C. Jing, Y. C. Shen, *et al.*, "Harnessing a multi-dimensional fibre laser using genetic wavefront shaping," *Light Sci. Appl.* **9**, 149 (2020).
13. K. Krupa, A. Tonello, B. M. Shalaby, *et al.*, "Spatial beam self-cleaning in multimode fibres," *Nat. Photonics* **11**, 237–241 (2017).
14. Z. W. Liu, L. G. Wright, D. N. Christodoulides, *et al.*, "Kerr self-cleaning of femtosecond-pulsed beams in graded-index multimode fiber," *Opt. Lett.* **41**, 3675–3678 (2016).
15. L. G. Wright, D. N. Christodoulides, and F. W. Wise, "Spatiotemporal mode-locking in multimode fiber lasers," *Science* **358**, 94–97 (2017).
16. T. Matyeevarunyoo, B. A. Malomed, and D. V. Skryabin, "Spatiotemporal dissipative solitons and vortices in a multi-transverse-mode fiber laser," *Opt. Express* **27**, 37364–37373 (2019).
17. U. Tegin, P. Wang, and L. V. Wang, "Real-time observation of optical rogue waves in spatiotemporally mode-locked fiber lasers," *Commun. Phys.* **6**, 60 (2023).
18. M. M. Nie, K. P. Jia, Y. J. Xie, *et al.*, "Synthesized spatiotemporal mode-locking and photonic flywheel in multimode mesoresonators," *Nat. Commun.* **13**, 6395 (2022).
19. B. Cao, C. X. Gao, K. W. Liu, *et al.*, "Spatiotemporal mode-locking and dissipative solitons in multimode fiber lasers," *Light Sci. Appl.* **12**, 260 (2023).
20. L. G. Wright, P. Sidorenko, H. Pourbeyram, *et al.*, "Mechanisms of spatiotemporal mode-locking," *Nat. Phys.* **16**, 565–570 (2020).
21. X. C. Gao, B. Cao, Y. H. Ding, *et al.*, "All-step-index-fiber spatiotemporally mode-locked laser," *Optica* **10**, 356–363 (2023).
22. U. Tegin, E. Kakkava, B. Rahmani, *et al.*, "Spatiotemporal self-similar fiber laser," *Optica* **6**, 1412–1415 (2019).
23. K. W. Liu, X. S. Xiao, Y. H. Ding, *et al.*, "Buildup dynamics of multiple solitons in spatiotemporal mode-locked fiber lasers," *Photonics Res.* **9**, 1898–1906 (2021).
24. Y. H. Ding, X. S. Xiao, P. Wang, *et al.*, "Multiple-soliton in spatiotemporal mode-locked multimode fiber lasers," *Opt. Express* **27**, 11435–11446 (2019).
25. Y. K. Guo, W. Lin, W. L. Wang, *et al.*, "Unveiling the complexity of spatiotemporal soliton molecules in real time," *Nat. Commun.* **14**, 2023 (2023).
26. H. Q. Qin, X. S. Xiao, P. Wang, *et al.*, "Observation of soliton molecules in a spatiotemporal mode-locked multimode fiber laser," *Opt. Lett.* **43**, 1982–1985 (2018).
27. K. W. Liu, X. S. Xiao, and C. X. Yang, "Observation of transition between multimode Q-switching and spatiotemporal mode locking," *Photonics Res.* **9**, 530–534 (2021).
28. X. S. Xiao, Y. H. Ding, S. Z. Fan, *et al.*, "Spatiotemporal period-doubling bifurcation in mode-locked multimode fiber lasers," *ACS Photonics* **9**, 3974–3980 (2022).
29. Z. Gao, T. Jiang, M. M. Zhang, *et al.*, "Breaking the speed limitation of wavemeter through spectra-space-time mapping," *Light. Adv. Manuf.* **4**, 13 (2024).
30. G. Pariente, V. Borot, O. Gobert, *et al.*, "Space-time characterization of ultra-intense femtosecond laser beams," *Nat. Photonics* **10**, 547–553 (2016).
31. J. C. Jing, X. M. Wei, and L. H. V. Wang, "Spatio-temporal-spectral imaging of non-repeatable dissipative soliton dynamics," *Nat. Commun.* **11**, 2059 (2020).
32. Y. Liu, T. T. W. Wong, F. Chen, *et al.*, "Compressed ultrafast spectral-temporal photography," *Phys. Rev. Lett.* **122**, 193904 (2019).
33. J. Y. Liang, L. R. Zhu, and L. H. V. Wang, "Single-shot real-time femtosecond imaging of temporal focusing," *Light Sci. Appl.* **7**, 42 (2018).
34. A. Ehn, J. Bood, Z. M. Li, *et al.*, "FRAME: femtosecond videography for atomic and molecular dynamics," *Light Sci. Appl.* **6**, e17045 (2017).
35. Y. K. Guo, X. X. Wen, W. Lin, *et al.*, "Real-time multispeckle spectral-temporal measurement unveils the complexity of spatiotemporal solitons," *Nat. Commun.* **12**, 67 (2021).
36. K. Goda and B. Jalali, "Dispersive Fourier transformation for fast continuous single-shot measurements," *Nat. Photonics* **7**, 102–112 (2013).
37. A. Mahjoubfar, D. V. Churkin, S. Barland, *et al.*, "Time stretch and its applications," *Nat. Photonics* **11**, 341–351 (2017).
38. D. K. Xing, M. Feng, C. C. Liu, *et al.*, "Spatiotemporal mode-locked fiber laser based on dual-resonance coupling long-period fiber grating," *Opt. Express* **31**, 7134–7143 (2023).
39. D. K. Xing, J. Y. He, P. Wang, *et al.*, "Transition between noise-like pulses and Q-switching in few-mode mode-locked lasers," *Opt. Express* **30**, 20076–20087 (2023).
40. Y. H. Ding, X. S. Xiao, K. W. Liu, *et al.*, "Spatiotemporal mode-locking in lasers with large modal dispersion," *Phys. Rev. Lett.* **126**, 093901 (2021).
41. Y. H. Wu, D. N. Christodoulides, and F. W. Wise, "Multimode nonlinear dynamics in spatiotemporal mode-locked anomalous-dispersion lasers," *Opt. Lett.* **47**, 4439–4442 (2022).
42. X. M. Liu, D. Popa, and N. Akhmediev, "Revealing the transition dynamics from Q switching to mode locking in a soliton laser," *Phys. Rev. Lett.* **123**, 093901 (2019).
43. X. M. Liu, X. K. Yao, and Y. D. Cui, "Real-time observation of the buildup of soliton molecules," *Phys. Rev. Lett.* **121**, 023905 (2022).
44. W. Y. He, G. X. Liu, G. X. Zhang, *et al.*, "Periodically tunable multimode soliton pulsation in a spatiotemporal mode-locked fiber laser," *Opt. Express* **32**, 4427–4435 (2024).
45. W. Y. He, G. X. Liu, J. W. Wu, *et al.*, "Spatiotemporal dual-periodic soliton pulsation in a multimode fiber laser," *Opt. Lett.* **49**, 1575–1578 (2024).
46. R. J. He, Z. Wang, Y. G. Liu, *et al.*, "Dynamic evolution of pulsating solitons in a dissipative system with the gain saturation effect," *Opt. Express* **26**, 33116–33128 (2018).
47. Q. Liang, H. J. Cao, J. J. He, *et al.*, "Spatial mode demodulation of multimode interference sensors by a "Fiber Camera";," *J. Lightwave Technol.* **42**, 7004–7009 (2024).